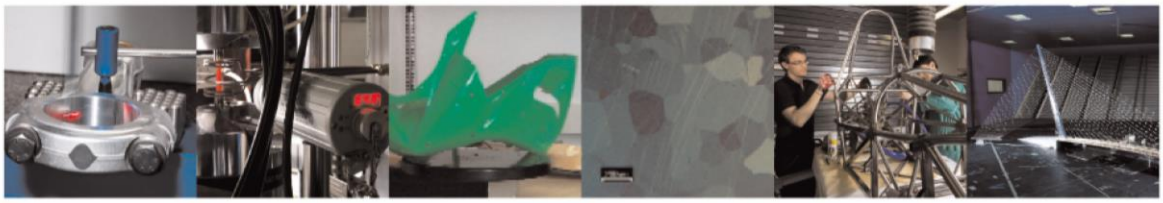

Influence of shielding gas flow on the µLMWD of biodegradable Mg alloy and permanent stainless steel for additive manufacturing of biomedical implants

Kaljevic, A.; Demir, A. G.

DIPARTIMENTO DI MECCANICA ■ POLITECNICO DI MILANO
via G. La Masa, 1 ■ 20156 Milano ■ EMAIL (PEC): pecmecc@cert.polimi.it
http://www.mecc.polimi.it
Rev. 0

Influence of shielding gas flow on the μLMWD of biodegradable Mg-alloy and permanent stainless steel for additive manufacturing of biomedical implants

Anna Kaljevic[1], Ali Gökhan Demir[1,*]

[1] Department of Mechanical Engineering, Politecnico di Milano, Via La Masa 1, 20156 Milan, Italy

*Corresponding author: aligokhan.demir@polimi.it

Influence of shielding gas flow on the μLMWD of biodegradable Mg-alloy and permanent stainless steel for additive manufacturing of biomedical implants

Anna Kaljevic[1], Ali Gökhan Demir[1,*]

[1] Department of Mechanical Engineering, Politecnico di Milano, Via La Masa 1, 20156 Milan, Italy

*Corresponding author: aligokhan.demir@polimi.it

Abstract

Wire feedstocks can be potentially used in additive manufacturing of customized biomedical implants. Micro laser metal wire deposition (μLMWD) can provide the dimensional resolution through the use of pulsed wave laser emission with small wire diameters (0.5 mm). Concerning the high reactivity of the biodegradable Mg-alloys the use of a wire feedstock can provide relatively safer option compared to powders. The local shielding of the process environment by an inert gas is of paramount importance for both biodegradable Mg alloys but also permanent implant materials such as stainless steel. In this work, the deposition feasibility via μLMWD of a biodegradable Mg alloy with Dy as the main alloying element (Resoloy) is studied along with a comparison with AISI 316, which has good processability. A shielding chamber was employed with oxygen content measurements during the process in order to reveal the oxygen take up or release during the process. An experimental study was employed to reveal the role of the process atmosphere on the process stability of Resoloy and AISI 316 deposits. Multiple layer deposits of the biodegradable Mg alloy were demonstrated. The results indicate that the highly reactive Mg alloy goes through a continuous oxygen intake and release during the deposition, while stainless steel mainly takes up oxygen from the environment. The deposition of multi-layered Resoloy specimens was proven to be possible to the less amount of surface oxide generated with the global shielding employed.

Keywords: biodegradable metals; Resoloy; directed energy deposition; laser metal wire deposition; atmospheric control

1. Introduction

Biodegradable implants are highly appealing for minimally invasive treatments. A biodegradable implant is expected to be resorbed by the body once it fulfils its duty. Biodegradable metals show better promise due to their higher mechanical strength compared to polymer and ceramic counterparts. Amongst the different metals, Mg, Zn and Fe are those that have been more widely studied for the production of biodegradable implants. The choice of the biodegradable alloy depends on the mechanical properties, absorption time, but also the implant type. Concerning the load bearing applications, biodegradable alloys combined with additive manufacturing techniques can open up to several improvements to the patient's treatment. Additive manufacturing provides the means to produce mass customized implants owing to the completely digital manufacturing approach. The implant location of the single patient can be acquired by CT-scans, designing the required shape and producing it directly [1].

Mg and its alloys have been widely studied in literature. Mg is an essential element found abundantly in the human body providing functions such as genome stabilization and being a cofactor for many enzymes. Mg has a density close to the human bone and has been shown to provide osteogenesis. Several alloys have been developed in literature improving the mechanical properties and the biodegradation behaviour. However, the manufacturability of these materials by metal additive manufacturing (AM) techniques remain an issue due to the same physical properties that render them desirable for the biomedical implants [1]. Mg has melting and vaporization temperatures at 915 K and 1363 K respectively. It is highly reactive with an oxidation enthalpy of -24.72 kJ/kg [2]. Hence, processing Mg alloys require specific attention concerning the energy input and the process atmosphere, when melting based processes are concerned.

Some of the most common metal AM processes are grouped as powder bed fusion (PBF) and directed energy deposition (DED) families. PBF concerns the use of an energetic beam, whether a laser or an electron-beam for selectively consolidating the powder feedstock in a layer-by-layer fashion. Laser powder bed fusion (LPBF) is arguably the most widely used metal AM process in the industry,

flexibly adapted to a larger variety of alloys. The processability of Mg and Zn alloys via LPBF is highly problematic due to the low vaporization temperatures and a very small gap between melting and vaporization points [3, 4]. Electron beam melting (EBM) is applied under vacuum to let the electrons focus on the powder bed. Such conditions lower further the vaporization point and can generate high process instability. For this reason in literature several groups have attempted to process biodegradable metals by LPBF. The processed Mg and Zn alloys required the manipulation of the process chamber in order to resolve the high vapour accumulation [5–9] or novel scan strategies [10]. The processability of Fe alloys by LPBF was found to be easier owing to much less volatility [11–13]. In all cases, the use of powder feedstock is complicated due to the safety issues. The size of the powder particles in LPBF (typically 15-50 μm) renders them potentially inflammable. From this point of view, the use of Mg-alloy powders is more problematic due to the high reactivity the material. Within the DED processes different energy sources (laser, electron beam, arc) can be combined with different feedstock types (powder, wire). Concerning the powder feedstock a laser beam (laser metal deposition, LMD) and an arc/plasma source (wire arc additive manufacturing, WAAM) can be combined sending the feedstock to the process region by the action of a vector gas. The high reactivity of the biodegradable alloys render these processes highly unreliable and unsafe. Instead the wire feedstock is intrinsically safer and it can be used combined with all the energy sources [14]. However, the electron beam requires vacuum and the arc/plasma sources are very large thermal sources reducing the precision required. Guo et al showed the advantage of wire and arc additive manufacturing process for producing multi-layered deposits with AZ31 Mg-alloy [15]. Although, the geometrical characteristics were not the main concern of the work, it showed the feasibility to use the Mg-alloy wires as feedstock in AM. The combination of the wire feedstock with a laser beam is laser metal wire deposition (LMWD) [16]. The process takes advantage of a laser beam, which is characterized by a well-concentrated energy source that can work in ambient atmosphere with a local shielding gas. The spatial resolution of this process has been further improved by means of a pulsed laser source and small wire diameters ($\leq$0.5 mm) towards the micro laser metal wire deposition (μLMWD)

process[17]. The process can be highly useful for safely producing Mg-alloy biodegradable implants with thin-walled features as an alternative to LPBF. Moreover the wire feedstock can provide a more economical alternative to the powder feedstock. Wire feedstock production through wire drawing enables better control over the final chemical composition and the overall yield is expected to be higher compared. In powder atomization only a fraction of the overall size distribution will be usable for the chosen process type such as LPBF or LMD. On the other hand, wire drawing of Mg-alloys is difficult due to low deformability of the material. Overall, the wire feedstock is expected to be economically convenient concerning the production and handing costs as well as the usage efficiency [18, 19]. With its main characteristics, the µLMWD process can be appealing especially for cranial and facial implants, which require thin walled complex geometries. However, being a DED process commonly applied in open atmosphere the µLMWD applies local gas shielding, which can be limiting to the processability of Mg-alloys. Surface oxidation can cause process instability due to its higher melting temperature and lower wettability [20].

Accordingly, this work assesses the processability of a novel and biodegradable Mg-alloy with rare earth elements within the alloy by µLMWD. In particular, the high reactivity of the alloy is tackled by means of a closed processing chamber with Ar flow and O_2 concentration measurement. The AISI 316 stainless steel was used for a less-reactive and processable material counterpart for comparison. Single and multi-layer tracks were produced and their geometries were analysed. In the light of these results multi-layered Resoloy thin-walls could be produced showing promise for future custom biodegradable implant manufacturing.

2. Materials and methods

2.1. Wire feedstock and substrate

The processability of the novel biodegradable Mg alloy was compared to a stainless steel with known processability. The material used as feedstock is a commercial magnesium alloy with dysprosium as the main alloying element (Resoloy, Fort Wayne Metals, Fort Wayne, Indiana, USA [21]). Resoloy

is employed in biomedical applications and has been specifically designed to be processed by lasers such as laser cutting for stent manufacturing [22]. The wire was produced by cold drawing and annealing and has a diameter of 0.5 mm. Magnesium substrates utilized were 2 mm thick sheets of AZ31 alloy, which were prepared by polishing with sandpaper and cleaning with acetone. Chemical composition of the materials, revealed by EDX analysis, is reported in Table 1.

Table 1 Chemical composition of the employed Magnesium alloy substrate and wire (wt%).

Material	Al	Zn	Zr	Nd	Eu	Dy	Mg
Resoloy wire	-	0.65	0.34	0.57	0.11	7.05	bal.
AZ31 plate	2.81	0.84	-	-	-	-	bal.

The material used as the stainless steel feedstock was AISI 316 wire, with a diameter of 0.5 mm. Stainless steel substrates were 5 mm thick hot rolled AISI 304 sheets, which were polished with sandpaper and cleaned in acetone. Chemical composition of both plate and wire, revealed by EDX analysis, is reported in Table 2**.**

Table 2 Chemical composition of the employed stainless steel substrate and wire (wt%).

Material	Si	Cr	Mn	Ni	Mo	Fe
AISI 316 wire	0.38	17.08	1.66	9.29	4.78	bal.
AISI 304 plate	0.47	18.19	1.64	7.62	-	bal.

In order to aid the discussion concerning the observed phenomenon Table 3 gathers the thermophysical parameters Resoloy and AISI 316.

Table 3 Thermo-physical parameters of the employed materials [23–26]

Property	Symbol	Resoloy	AISI 316
Density	ρ [kg/m^3]	1830	7880
Specific heat (solid)	c_{p_S}[J/kg K]	993 (Mg)	500 (Fe)
Specific heat (liquid)	c_{p_L}[J/kg K]	1340 (Mg)	820 (Fe)
Melting temperature	T_m [K]	915 (Mg)	1470
Vaporization temperature	T_v [K]	1363 (Mg)	3273
Latent heat for melting	L_m [kJ/kg]	368.4 (Mg)	260 (Fe)
Latent heat for vaporization	L_v [kJ/kg]	5241.5 (Mg)	6500 (Fe)
Enthalpy of oxidation	ΔH [kJ/kg]	-24.72 (Mg)	-4.66 (Fe)
Viscosity at melting temperature	η (mPa s)	1.25 (Mg)	6

2.2. μLMWD with controlled process atmosphere

A custom µLMWD system operating in controlled processing atmosphere was employed throughout the study. The system consisted of an automated laser welding station (Powerweld HL 124P from Trumpf, Ditzingen, Germany), a flash pumped Nd:YAG laser source, a custom build wire feeding system and inert chamber. The laser source provided 120 W maximum average power with pulse durations (τ) in µs to ms regime and a maximum pulse repetition rate (*PRR*) at 300 Hz. The maximum pulse energy (*E*) and the maximum peak power (P_{peak}) were of 50 J and 5 kW respectively. The laser beam was transported from the source to the workstation by fiber delivery, featured by a 0.4 mm diameter and 200 mm collimating and 150 mm focal lenses, so that the minimum spot diameter achievable is 0.3 mm. The main specifications of the laser system are summarized in Table 4.

Table 4 Main specifications of the laser system.

Laser parameter	**Value**
Emission wavelength, λ	1064 nm
Max average power, P_{avg}	120 W
Max peak power, P_{peak}	5 kW
Max pulse energy, E	50 J
Pulse duration, τ	0.3 – 20 ms
Pulse repetition rate, *PRR*	1 – 300 Hz
Beam parameter product, *BPP*	16 mm·rad
Minbeamdiameter,d_0	300 µm

Substrates were mounted on the positioning system that provided two linear and a rotational axes. The laser head could be moved along a third axis to maintain the focal point at the desired height. The wire feed rate (*WFR*) was regulated via a LabVIEW interface and synchronizing the laser emission at the start of each new layer. A custom built process chamber was fitted the µLMWD system, as reported in Figure 1. Ar was used as the inert gas, which was flown to the chamber with controlled gas flow rate. The oxygen concentration inside the chamber was monitored through an oxygen sensor based on optical fluorescence quenching (SST LuminOx Flow-through Optical Oxygen Sensor, Coatbridge, UK). The sensor was characterized by a measurement range of 0-25 vol%, 0.01 vol.% resolution and a declared accuracy of <0.5 vol.%.

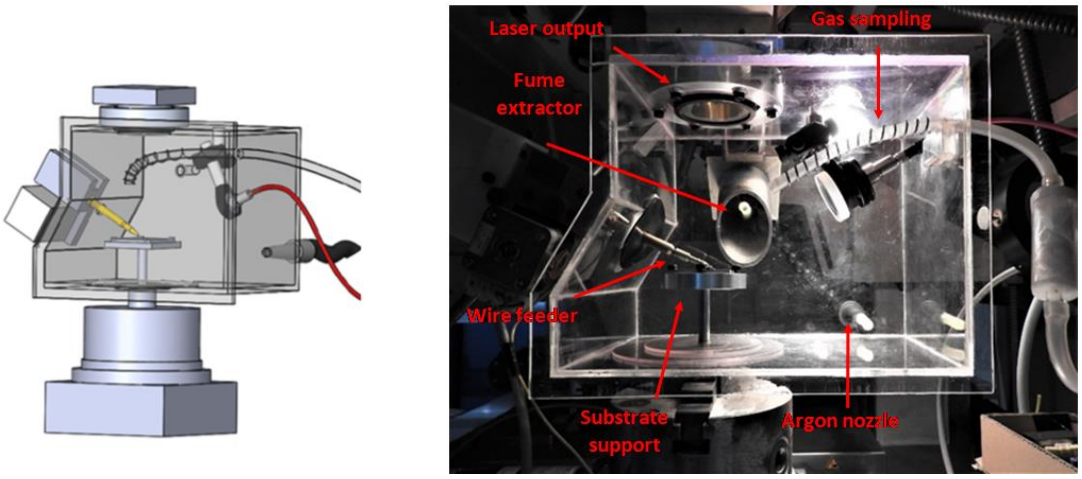

Figure 1 (a) Design of the µLMWD in inert chamber system and (b) photograph of the built system

The inertization of the process chamber was characterized by selecting three different levels of Ar flow rate and monitoring the evolution of the oxygen concentration during the purging process. The oxygen concentration evolution during the purging phase is reported in Figure 2. It can be seen that the O_2 concentration could be lowered below 1 vol% at higher flow rates

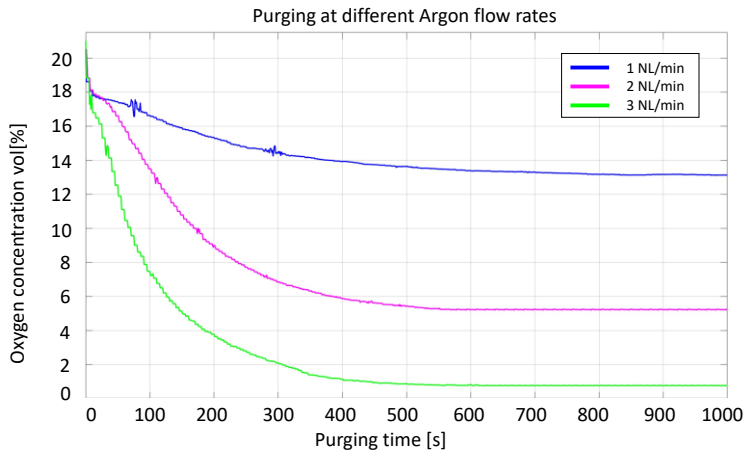

Figure 2 Oxygen concentration evolution during the purging phase.

2.3. Experimental procedure

The processability windows of Resoloy and AISI 316 were studied in parallel to allow for a comparison. Preliminary experiments, not reported here for brevity, showed that the energy levels

required for the Resoloy wire were significantly lower compared to AISI 316. The high energy levels generated complete vaporization of the Resoloy wire, while the low energy levels generated insufficient melting on AISI 316. Hence, the feasibility windows were sought within different laser energy levels for the two materials with the aim to establish stable deposition conditions different argon flow rate levels. Single tracks with 15 mm length were deposited. Ar flow rate (F [NL/min]) and laser energy (E [J]) were varied. Flow rate levels tested for both materials were 0 NL/min, 1 NL/min, 2 NL/min and 3 NL/min, while laser energy levels differed between AISI 316 and Resoloy due to thermo-physical properties of the two. AISI 316 was processed with laser energy values from 8.8 J to 14.4 J, while for Resoloy the energy levels were varied in the range between 2.0 J and 5.0 J. The other process parameter were selected according to previous works [17, 27, 28], and are reported in Table 5. At this stage, each run was analysed from the process quality point of view, since conditions generating stable deposition process were sought.

Table 5. Fixed process parameters selected during the during single track deposition tests.

Fixed process parameters	**Resoloy**	**AISI 316**
Wire diameter, d_w	0.5 mm	0.5 mm
Laser spot diameter, d_s	0.90 mm	0.85 mm
Pulse duration, τ	6.0 ms	7.4 ms
Pulse repetition rate, *PRR*	9 Hz	7 Hz
Wire feed rate, *WFR*	220 mm/min	260 mm/min
Transverse speed, v	60 mm/min	162 mm/min
Wire feeding angle, α	30°	30°
Wire feeding direction	Frontal	Frontal
Focal point, f	0 mm	0 mm
Height increment, Δz	0.3 mm	0.3 mm
Varied process parameters	**Resoloy**	**AISI 316**
Laser energy, E [J]	3.0, 3.6, 4.0	9.9, 11.4, 12.9
Gas flow rate, F [NL/min]	1, 2	0, 1, 3
No of layers, n	1, 3	1, 5

The experimental plan was designed around the feasibility window, which was determined as result of the first step. Laser energy and gas flow rate were varied, since the effect of the two on deposition was sought. Number of layers deposited was a variable parameter as well, as it is related to the stability of the process during its evolution. During the tests the oxygen concentration in the chamber was measured.

2.4. Characterization

Samples were cut and cold-mounted in order to not induce any heat input during the hot mounting process. The specimens were ground and polished following conventional metallographic preparation techniques.

2.4.1. Deposit geometry

Optical microscopy images of specimen sections were analysed through image processing software. Width and height were measured respectively as the highest value of width and height among the cross section and are indicated with *w* and *h.* The average aspect ratio of the layers is defined as the average ratio between height and width and is indicated with *AR*, and calculated as

$$AR = \frac{h}{wn} \tag{1}$$

where *n* is the number of layers deposited. Higher *AR* values are more desirable for the µLMWD process in order to reduce the lateral spread of the material and hence increase deposit width. Moreover, this parameter indicates the morphological changes induced by the process parameters. While the influence of laser energy and pulse duration may be more intuitive, the influence of the process atmosphere requires further attention in order to assess the changes in the process conditions.

2.4.2. Material microstructure and microhardness

A preliminary analysis on the Resoloy deposits was carried out to reveal the feasibility of producing sound parts with the µLMWD method. Chemical etching was employed to reveal the microstructure of the cross sections. Resoloy was etched with a solution composed of 90 ml C_2H_5OH and 10 ml HNO_3 for 60 seconds. SEM imaging was used to investigate the microstructure of multi-layered Resoloy sample. Microhardness tester was used for characterization of Resoloy multi-layer sample, selecting load test at 50 gf and dwell time of 15 seconds. On the other hand, AISI 316 was etched with Nital for 60 seconds to reveal the melt structure. A detailed analysis on AISI 316 material microstructure was not carried out as it was only used for a comparison in terms of a material with known process stability and material characteristics [29].

2.4.3. Variation of oxygen concentration during the process

The difference between measured oxygen concentrations at the process start, $O_{2,start}$, and end, $O_{2,end}$ was measured throughout the experiments, defined as

$$\Delta O_2 = O_{2,start} - O_{2,end} \quad (2)$$

Oxygen concentration was not monitored during 0 NL/min flow rate experiments, since these were performed with open chamber.

3. Results and discussion

3.1. Process feasibility windows

Conditions generating stable deposition process were sought during preliminary experiments. Figure 3 reports a series of examples showing the stable and unstable deposition types. Results are visually represented as a feasibility map, as reported in Figure 4. Concerning the Resoloy wire, the process was found to be more susceptible to the internal turbulence that may be formed due to the gas flow. Indeed, with small wire diameters mechanical stability of the wire flow can be an important process destabilizer. Resoloy, being a Mg-alloy with smaller elastic modulus compared to the stainless steel, was found to be easily bent and vibrated by the high gas flow rates. During the experiments it was observed that working with high flow rate made the samples also thinner. Hence, successive layers had to be deposited on these narrow tracks introducing a further complication in the positioning of the wire tip. The effect on the process is that the wire tip escapes from the processing zone, making the deposition process unfeasible. At lower gas flow rates, excessive surface oxidation was observed by the visible darkening of the tracks. The pulse energy required to successfully produce Resoloy tracks is also limited and the range changes with the gas flow rate. With low laser energy at higher flow rates stubbing is observed. Stubbing phenomenon is related to insufficient energy to melt the material. At high energy values and low gas flow rates the material vaporization was stronger. These two factors indicate that the high reactivity of the Mg-alloy plays a key role on the energy balance despite the restricted 2 to 5 J pulse energy input provided. The oxidation enthalpy is expected to

contribute to the process at low flow rates avoiding stubbing with low pulse energy and moving towards vaporization at high energy levels.

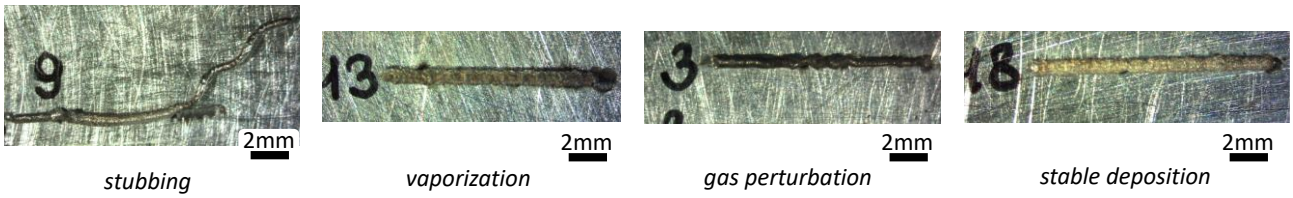

Figure 3 Stable and unstable conditions observed during the Resoloy experimental runs.

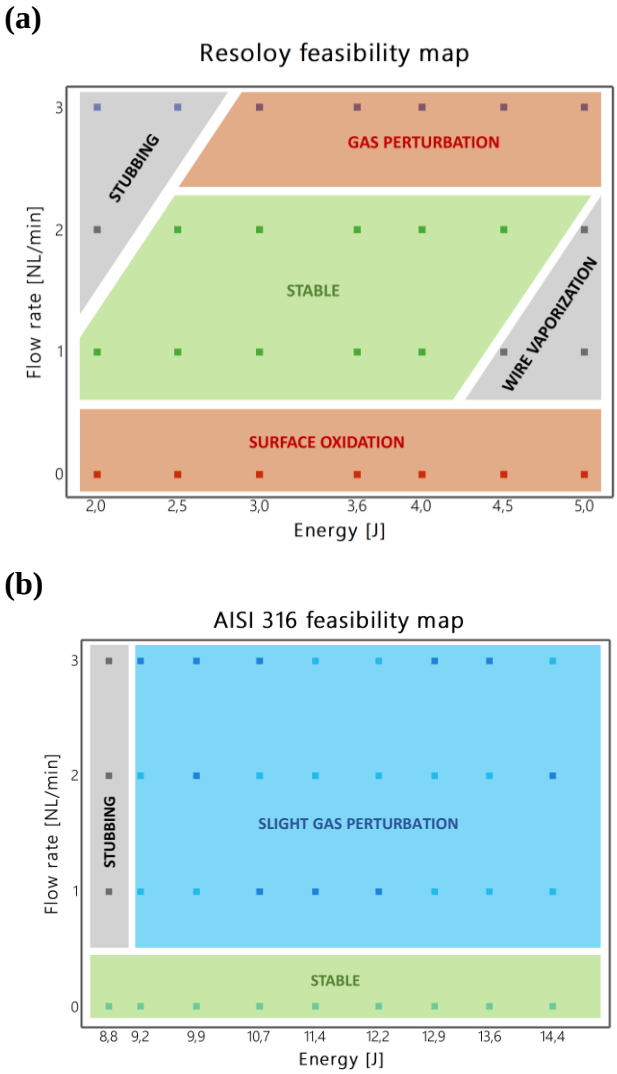

Figure 4 Feasibility maps for (a) Resoloy and (b) AISI 316 processability

Concerning AISI 316, a stable process was achieved for all the laser energy values tested, when the process was performed in atmospheric conditions. Two qualitative regions are identified when deposition was carried out in the inert chamber. For the lowest laser energy values, stubbing occurred frequently working in the inert chamber, while at intermediate and high energy values deposition was

much more stable with stubbing occurring rarely. This can be attributed to the melt pool instability due to the turbulent gas flow in the chamber, which may occasionally pull the wire feedstock out of the designed path.

3.2. Deposit morphology and microstructure

Figure 5 shows the morphology of single and multi-layered Resoloy and AISI 316 deposits obtained in the experimental study. It can be seen that the dilution of the Resoloy samples to the AZ31 baseplate is limited. On the other hand, the multiple layers appear to have adhered correctly. Concerning the AISI 316 deposits, the dilution can be much higher as shown in Figure 5. Within the studied parameter range of AISI 316, keyholing could occur and increase penetration to the baseplate as well as the previous layers. The chosen process parameter ranges kept Resoloy in a closer to a conduction mode deposition, avoiding excessive vaporization yet generating a limited or missing dilution. The shape of the deposits also indicate that Resoloy wires tend to have a scares wetting with the baseplate. To increase the dilution with the baseplate, the laser energy could be increased. However, with increased energy levels towards the values outside the feasibility window the wire was lost to complete to evaporation. On the other hand, the energy levels employed in the experimental plan were sufficient to provide complete bonding between the successive layers. Although the initial adherence to the baseplate was not continuous, the use of µLMWD for producing freestanding Resoloy components can be feasible. Concerning adding features to existing Mg-alloy parts, the use of µLMWD may be limited to the locally reduced dilution. The smaller contact angle with the substrate observed with AISI 316 suggests that the material could wet the substrate well. With multiple layers the jagged edges of the Resoloy deposits indicate that scarce wetting may persist along the successive layers. The smoother edges of AISI 316 indicate a stable and smoother deposition along the build direction. This differences in the wetting behaviour can be attributed to the oxide formation. The MgO on the substrate and also on the deposited layers can inhibit the wetting of Mg alloy. The melting temperature of MgO (3098 K) compared to Mg (905 K) is approximately

3.5 times higher [30]. During the µLMWD process the feedstock should melt and transfer heat to the base plate in order to melt it. With limited energy input in order to avoid excessive vaporization, the removal of the MgO layer during the process becomes even more difficult. While a scarce adhesion to the substrate may hinder the anchorage of the deposited layers, a scarce adhesion between the layers results in no deposition. These observations further underline the necessity of controlling the atmosphere during the processing of Mg alloys. Main effects and interaction plots of aspect ratio (AR) measured on the two materials are reported in Figure 6. Main effects plot of *AR* shown for both AISI 316 and Resoloy a predominant influence of flow rate. Increasing the flow rate, *AR* is higher, so samples are thinner. On the contrary, laser energy plays an opposite role. As shown in previous works, higher laser energy leads to wider and shorter tracks [17, 31]. From the evaluation of interaction plots, it can be predicted that there is a significant interaction between layers and flow rate parameters on AISI 316, while other interactions seem to have no effect on the aspect ratio.

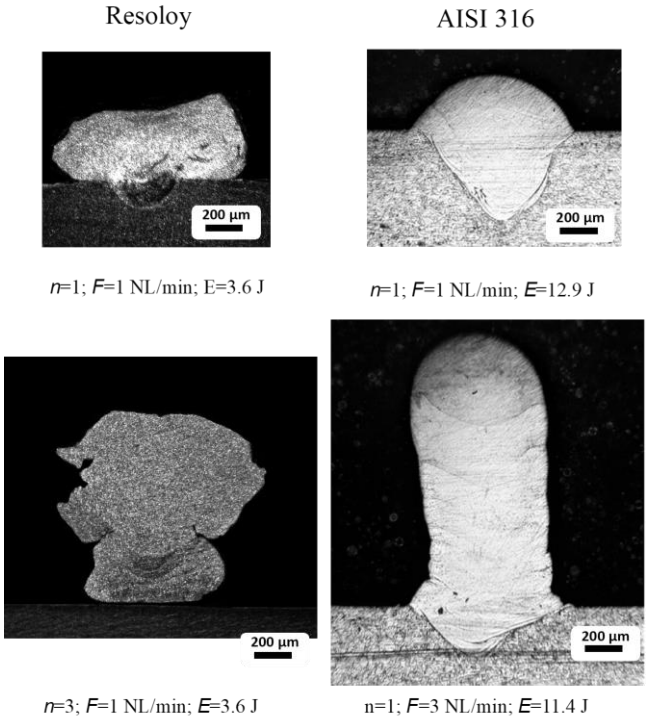

Figure 5 Example micrographs of the single and multi-layered deposits obtained with Resoloy and stainless steel.

The analysis of variance (ANOVA) table resulting from the design analysis is reported in Table 6. Statistical significance was evaluated with a *p*-value at 5%. Statistical analysis on *AR* for Resoloy

sample shows instead that only flow rate and layers were significant on *AR* response. Considering AISI 316, it appears that both energy, flow rate and layers are significant, while the only interaction that affects the tracks geometry is the combination between flow rate and layers. Resoloy responds similar to AISI 316 considering the influence of flow rate and laser energy on the deposition geometry. An increase in the input energy makes tracks wider and shorter. An increase of argon flow rate, and so the consequent decrease in oxygen concentration inside the chamber, leads to thinner samples. Moreover, sample surface appears to be smooth when process is performed at high flow rate. This can be attributed to a decrease in the overall energy content, as less oxidation must have occurred. Accordingly, higher flow rates tend to have an effect similar to a lower laser energy. As already discussed, the higher flow rates should be considered along with the mechanical behaviour of the wire. While AISI 316 is more rigid and stands turbulences induced by the gas flow, Resoloy is highly susceptible to gas perturbations. This phenomenon makes it difficult to process Resoloy by µLMWD process at very low oxygen concentrations with the current gas flow arrangement.

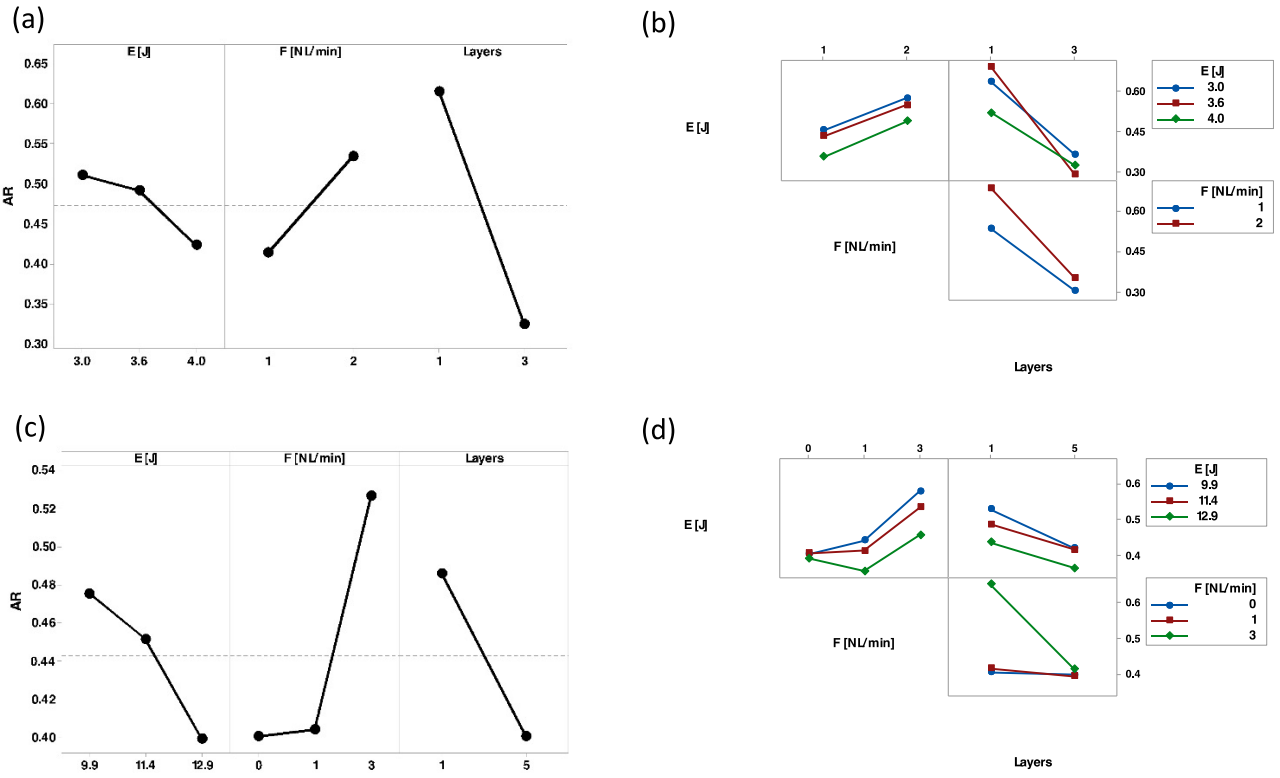

Figure 6 (a) Main effects and (b) interaction plots of aspect ratio (*AR*) obtained on Resoloy. (c) Main effects and (d) interaction plots of aspect ratio (*AR*) obtained on AISI 316

Table 6. Statistical significance of process parameters on AISI 316 and on Resoloy aspect ratio (*AR*) depicted by corresponding *p*-values. The *p*-values of statistically significant parameters and interactions are depicted in italic.

Source	***AR* Resoloy**	***AR* AISI 316**
E [J]	0.133	*0.002*
F [NL/min]	*0.006*	*0.000*
Layers	*0.000*	*0.000*
E [J] x F [NL/min]	0.776	0.392
E [J] x Layers	0.056	0.838
F [NL/min] x Layers	0.282	*0.000*
E [J] x F [NL/min] x Layers	0.082	0.533

3.3. Oxygen release or intake during the process

Interval plots of ΔO_2 measured for Resoloy and AISI 316 are reported in Figure 7. A positive value of ΔO_2 means that the initial oxygen concentration is higher than the final one, hence, oxygen available in the atmosphere is consumed. On the contrary, a negative ΔO_2 value represents a situation in which during the process, oxygen is generated, most likely released from the feedstock. Prior to a detailed analysis, the resolution and the declared accuracy of the measurements should be considered. For a sensible change in the oxygen content in the atmosphere it can be assumed that the variation should be reasonably higher than the measurement accuracy of the device. In the absence of a detailed and robust analysis of the measurement error, an average variation of ±1 vol.% was considered a remarkable change.

Overall the plots show a higher change of ΔO_2 of when multi-layer depositions are concerned. Considering that process duration is longer for multi-layer manufacturing, the oxygen intake or release is expected to be more marked. Laser energy instead, does not appear to affect the oxygen concentration variation. It should be noted that the oxygen content variations with single layers are limited around ±0.5 vol%. A sensible difference in the processing atmosphere with $|\Delta O_2| \geq 1$ vol.% is observed during the processing of multiple layers with an influence of the flow rate. During the multi-layer depositions, the materials show remarkably different behaviour. An increase of the O_2 content is observed for Resoloy during multiple layer depositions. This indicates that the material tends to release O_2 during the process. This can be attributed to a cyclic formation and destruction of the oxide

layer during the process. Due to the very high affinity of the material to oxidation, the wire feedstock is also expected to provide the oxygen to the process chamber. At low flow rates during the multi-layer deposition, the material is expected to release the O_2 from the wire surface to the chamber increasing the oxygen concentration. The use of higher flow rate appears to purge the oxygen more easily and go towards a balanced condition concerning the oxygen intake and release. AISI 316 at multiple layer deposition shows a similar behaviour concerning the effect of the flow rate. However, at higher flow rates the oxygen appears to be absorbed by the deposited material. The surface oxide of AISI 316 is expected to be much thinner and hence oxygen release from the material should be much more limited compared to Resoloy. With higher flow rate and hence lower initial oxygen content, the balance is towards oxygen intake rather than release to the environment. The results show that the higher reactivity of the feedstock material implies a higher degree of oxygen release to the processing environment, which can be better purged with higher flow rates.

(a)

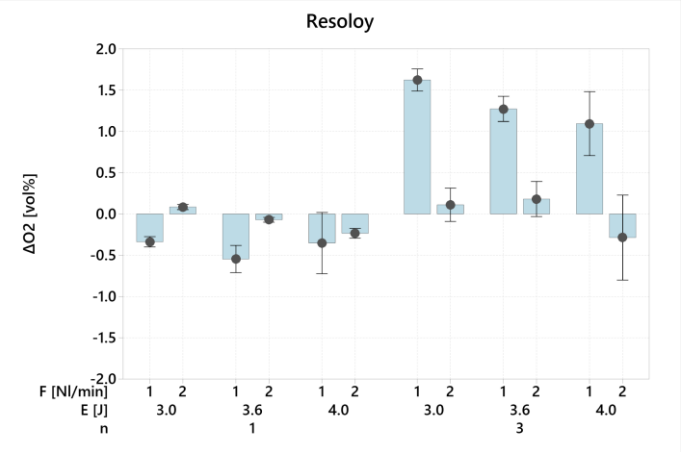

(b)

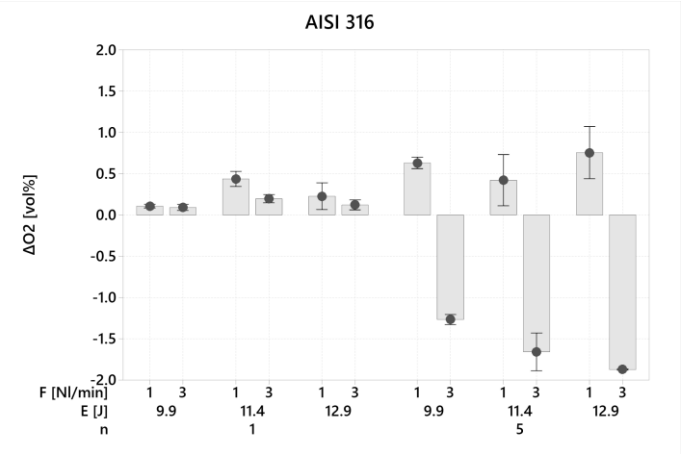

Figure 7 Interval plots of ΔO_2 for Resoloy (a) and for AISI 316 (b) (error bars represent standard error).

4. Demonstration of multi-layered Resoloy deposition and preliminary characterization

In the light of the processability study, a Resoloy thin wall was manufactured selecting the most suitable process parameters. The choice of process parameters was driven both by results of previous experimental campaign and by stability of the process. Laser energy was fixed at 4.0 J. Best aspect ratio as achieved with the highest flow rate, however Resoloy wire is highly prone to vibrate and move away from the processing zone due to gas flow. A compromise was found at flow rate of 1 NL/min. Eight layers were deposited for further analysis of material properties. Figure 8 shows the cross section of the specimen. The thin-wall is characterized by highly rough edges and a jagged

profile as previously observed. Mg has a lower viscosity at melting temperature compared to AISI 316. Moreover, the preservation of large melt pools due to low cooling rates can occur with Mg alloys, which has been already observed in LPBF of WE43 Mg alloy [5]. Combined with a scares wettability, these factors should have contributed in a more accentuated lateral melt flow, generating the jagged profile. Such profile has an effect on the surface quality, but can also be problematic for the densification of larger components with multiple tracks on the same layer. It can be expected that with overlapping tracks on the same plane some partial remelting of the previously deposited tracks should occur providing a smoother deposit along the layer. Besides the deposit profile, a fully dense pore-free material with no evidence of cracks is seen. It can be stated once stable processing conditions are achieved, µLMWD can provide deposits free of internal defects.

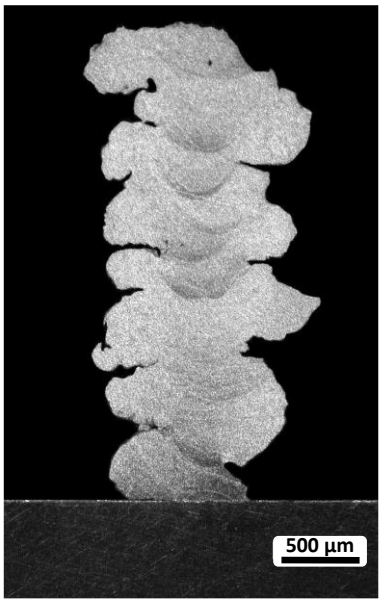

Figure 8 Resoloy thin wall cross section, showing the layer formation along the build direction (vertical direction in the image). The image confirms full melting and material consolidation between layers with an irregular surface formation.

Metals produced by additive manufacturing processes commonly show distinct microstructures compared to their conventional counterparts. In particular, metals produced by directed energy deposition processes generally feature microstructural anisotropy, with epitaxial grain growth in the building direction [16, 32]. Such anisotropy has been found to be more limited for µLMWD due to the pulsed wave emission of the laser. In µLMWD the laser pulses act on solid material between rather than working with a continuous melt flow. This results in a limited heat input and remelting

between the consecutive layers [33]. Figure 9 reports the microstructure of µLMWD processed Resoloy. The analysis suggests an equiaxial grain growth along the build direction, which is expected to be the consequence of uniform thermal profiles generated during the process. As the feedstock wire diameter is smaller than the laser spot diameter the heat input is more homogenous along the wire radius. Among the matrix, Dy precipitates were found, as reported in Figure 9. Such precipitates with increased content of Dy, that appear as bright phases, have been found in literature in similar alloys [34]. The µLMWD process generates an evenly distributed network of these precipitates similar to what has been previously observed with Al-12Si alloy[33]. Further research is required to fully characterize the obtained microstructure.

EDX analysis revealed that alloying elements concentrations profile is stable along the build direction, as reported in Figure 10.a. A decrease of the magnesium content in the thin wall with respect to the wire is expected to be due to Mg depletion during the process, as consequence of its lower vaporization temperature. The oxygen intake is also crucial for the functioning and biodegradation behaviour of the implant. an accurate measurement of the oxygen content in the deposited material could not be made with EDX due to its limited resolution with lighter elements. Future works should better assess the influence of the processing conditions on the material chemical composition.

The thin wall sample shows a stable profile along the build direction in terms of mechanical properties as reported in Figure 10.b. The microhardness values range between 79 and 89 HV, being lower than the average feedstock wire microhardness of 107 HV. This can be attributed to the change of alloy composition as well as the microstructure that occurs during the manufacturing process.

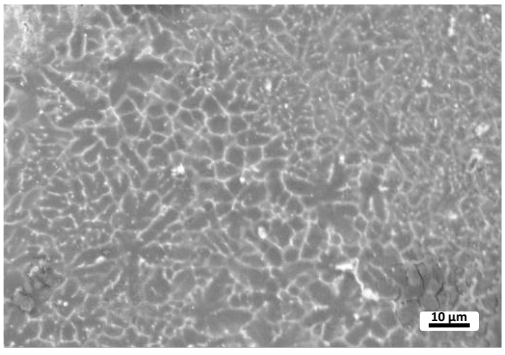

Figure 9 Microstructure of the Resoloy thin-wall.

(a)

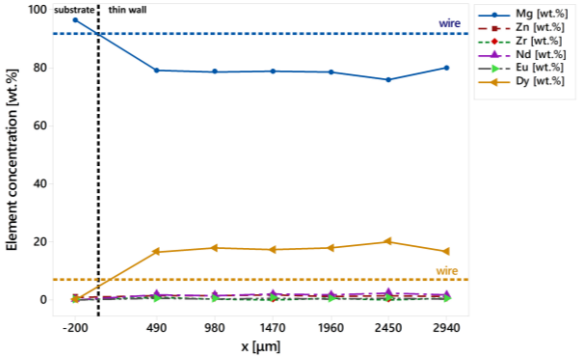

(b)

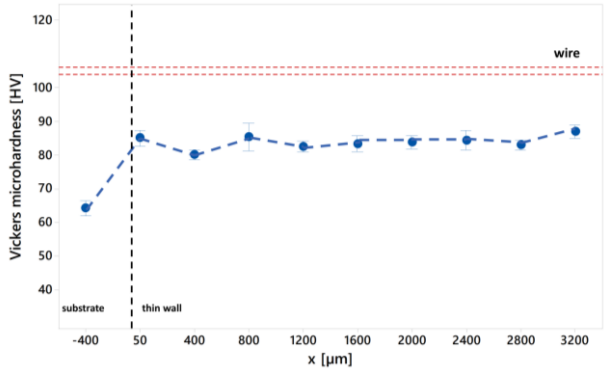

Figure 10 Element concentration profile along the building axis x (a); Microhardness profile along the building axis x, where error bars represent standard error

Table 7 compares the microhardness values measured for laser based additive manufacturing processes employing different magnesium alloys. It can be seen that mechanical properties are comparable to laser powder bed fusion (LPBF) processed Mg alloys. Table 8 reports Vickers hardness values of biodegradable alloys compared to human bone. It can be seen that the hardness of µLMWD produced Resoloy is comparable to pure Mg processed by LPBF. The microhardness values are comparable to those of Mg alloys with Al-Zn content. Although LPBF is expected to induce a faster cooling, combined with the alloying constituents and the fine microstructure µLMWD processed Resoloy appears to provide promising mechanical properties. The relatively higher microhardness compared to the human bone be disadvantageous in load bearing applications. In such conditions

geometrical designs, the use of lattice structures can be employed, requiring further attention on the geometrical capabilities of the µLMWD process.

Table 7. Summary of Vickers microhardness (HV) values of magnesium alloys produced by laser additive processes

Magnesium alloy	Hardness (HV)	Process	Reference
Mg	75 ± 15	LPBF	[4]
Mg-9Al	76 ± 10	LPBF	[35]
AZ91D	93 ± 7	LPBF	[36]
ZK60	78	LPBF	[37]
ZK60	80 ± 19	LPBF	[38]
Resoloy	83.4 ± 5	µLMWD	Current study

Table 8. Summary of Vickers microhardness (HV) values of biodegradable metals produced by different manufacturing methods compared to the human bone

Material	µLMWD	LPBF	Cast	Wrought	Reference
Pure Fe	NA	150 ± 6.5	130 (Mild steel)	150 (Mild steel)	[39]
Pure Zn	NA	45 ± 5.4	NA	34 ± 2	[40]
Pure Mg	NA	78 ± 8.2	30 ± 2	41 ± 2	[41]
Resoloy	83.4 ± 5	NA	NA	107	Current study
Human bone			40 - 79		[3]

5. Conclusions

In this work, the influence of processing atmosphere on µLMWD of Resoloy as a Mg-based biodegradable alloy and AISI 316 as a permanent bioimplant material was assessed. While µLMWD provided the advantage of using the wire feedstock, which provides an intrinsically safer deposition process for Mg alloys, the use of global gas shielding was required. The comparative analysis between the materials provided insights to process mechanisms as well as the development of future biodegradable and permanent implants. The main results are summarized as follows.

- The gas flow rate influenced process stability by means of determining the oxidation behaviour, but also wire instabilities due to the flow within the process chamber.
- The Mg-alloy was more sensitive to the process atmosphere as the processing conditions vary significantly within a limited pulse energy range (2-5 J) compared to the stainless steel (9-15J).

- The oxygen content measurements showed that the during the processing of AISI 316 oxygen pickup by the material can occur. Hence, energy may be added to the process through the oxidation enthalpy. On the other hand with Resoloy the oxygen content could increase during the process. This indicates a cyclic behaviour of oxidation of the formed layers and release of the oxides at the successive ones during the process.
- Despite the high sensitivity of the material to oxidation and gas perturbances, multi-layered Resoloy specimens could be deposited showing homogenous microstructure and hardness profile. The resultant microhardness, which is lower than that of the initial wire, is the combination of the new elemental composition and the cooling rate of the process.
- µLMWD can be an alternative metal additive manufacturing process for highly reactive Mg-alloys as it provides fully dense and crack free deposits with a relatively simpler machine architecture, and a feedstock that is advantageous in terms of safety and cost. The geometric fidelity requires further attention to match the capabilities of competing processes mainly of LPBF.

In addition to these results, the present work showed a systematic analysis to investigate the processability of these new generation of biodegradable alloys based on Mg by additive manufacturing. Although the geometrical accuracy is far from the desired, the results pave way for indicating the process requirements from the process-machine perspective. One key factor is related to the design of the process gas nozzle and chamber, which should require further attention. Feedstock material design also should also take the chemical variations into account increasing the Mg content to balance its loss. The wires should also be designed in chemistry and heat treatments for producing mechanically stable precursors for the process.

Acknowledgements

The authors wish to express their gratitude to Fort Wayne metals for providing the Resoloy wires.

Declarations

Funding

The Italian Ministry of Education, University and Research is acknowledged for the support provided through the Project “Department of Excellence LIS4.0—Lightweight and Smart Structures for Industry 4.0”.

Authors contributions

AK carried worked on the development of the experimental setup and data acquisition. AGD conceptualized and supervised the research and provided the resources. Both the authors contributed to the data analysis and writing.

Conflicts of interest

The authors declare no competing interests.

Data availability

The data will be shared upon request.

Ethics approval

Not applicable

Consent to participate

Not applicable

Consent for publication

Not applicable

References

1. Carluccio D, Demir AG, Bermingham MJ, Dargusch MS (2020) Challenges and Opportunities in the Selective Laser Melting of Biodegradable Metals for Load-Bearing Bone Scaffold Applications. Metall Mater Trans A Phys Metall Mater Sci. doi: 10.1007/s11661-020-05796-z
2. Gökhan Demir A, Previtali B (2014) Comparative study of CW, nanosecond- and femtosecond-pulsed laser microcutting of AZ31 magnesium alloy stents. Biointerphases 9: . doi: 10.1116/1.4866589
3. Ng CC, Savalani M, Man HC (2011) Fabrication of magnesium using selective laser melting technique. Rapid Prototyp J 17:479–490 . doi: 10.1108/13552541111184206
4. Ng CC, Savalani MM, Lau ML, Man HC (2011) Microstructure and mechanical properties of selective laser melted magnesium. Appl Surf Sci 257:7447–7454 . doi: 10.1016/j.apsusc.2011.03.004
5. Zumdick NA, Jauer L, Kersting LC, et al (2019) Additive manufactured WE43 magnesium: A comparative study of the microstructure and mechanical properties with those of powder extruded and as-cast WE43. Mater Charact 147:384–397 . doi: 10.1016/j.matchar.2018.11.011
6. Jauer L, Jülich B, Voshage M, Meiners W (2015) Selective laser melting of magnesium alloys. Eur Cells Mater 30 Suppl.3:1
7. Wen P, Voshage M, Jauer L, et al (2018) Laser additive manufacturing of Zn metal parts for biodegradable applications: Processing, formation quality and mechanical properties. Mater Des 155:36–45 . doi: 10.1016/J.MATDES.2018.05.057
8. Montani M, Demir AG, Mostaed E, et al (2017) Processability of pure Zn and pure Fe by SLM for biodegradable metallic implant manufacturing. Rapid Prototyp J 23: . doi: 10.1108/RPJ-08-2015-0100
9. Demir AG, Monguzzi L, Previtali B (2017) Selective laser melting of pure Zn with high density for biodegradable implant manufacturing. Addit Manuf 15:20–28 . doi: 10.1016/j.addma.2017.03.004
10. Guaglione F, Caprio L, Previtali B, Demir AG (2021) Single point exposure LPBF for the production of biodegradable Zn-alloy lattice structures. Addit Manuf 102426 . doi: 10.1016/j.addma.2021.102426
11. Carluccio D, Demir AG, Caprio L, et al (2019) The influence of laser processing parameters on the densification and surface morphology of pure Fe and Fe-35Mn scaffolds produced by selective laser melting. J Manuf Process 40:113–121 . doi: 10.1016/j.jmapro.2019.03.018
12. Carluccio D, Bermingham M, Kent D, et al (2019) Comparative Study of Pure Iron Manufactured by Selective Laser Melting, Laser Metal Deposition, and Casting Processes. Adv Eng Mater 21: . doi: 10.1002/adem.201900049
13. Carluccio D, Xu C, Venezuela J, et al (2020) Additively manufactured iron-manganese for biodegradable porous load-bearing bone scaffold applications. Acta Biomater 103:346–360 . doi: 10.1016/j.actbio.2019.12.018
14. Ding D, Pan Z, Cuiuri D, Li H (2015) Wire-feed additive manufacturing of metal components: technologies, developments and future interests. Int J Adv Manuf Technol 81:465–481 . doi: 10.1007/s00170-015-7077-3
15. Guo J, Zhou Y, Liu C, et al (2016) Wire arc additive manufacturing of AZ31 magnesium alloy: Grain refinement by adjusting pulse frequency. Materials (Basel) 9: . doi: 10.3390/ma9100823
16. Motta M, Demir AG, Previtali B (2018) High-speed imaging and process characterization of coaxial laser metal wire deposition. Addit Manuf 22:497–507 . doi: 10.1016/j.addma.2018.05.043
17. Demir AG (2018) Micro laser metal wire deposition for additive manufacturing of thin-walled structures. Opt Lasers Eng 100:9–17 . doi: 10.1016/j.optlaseng.2017.07.003
18. Cunningham CR, Wikshåland S, Xu F, et al (2017) Cost Modelling and Sensitivity Analysis of Wire and Arc Additive Manufacturing. Procedia Manuf 11:650–657 . doi: 10.1016/j.promfg.2017.07.163
19. Jafari D, Vaneker THJ, Gibson I (2021) Wire and arc additive manufacturing: Opportunities and challenges to control the quality and accuracy of manufactured parts. Mater Des 202:109471 . doi: 10.1016/j.matdes.2021.109471
20. Demir AG, Previtali B, Biffi CA (2013) Fibre laser cutting and chemical etching of AZ31 for manufacturing biodegradable stents. Adv Mater Sci Eng 2013: . doi: 10.1155/2013/692635
21. Stekker M, Hort N, Feyerabend F, et al (2016) Resorbable stents which contains a magnesium alloy. 1–31

22. Griebel AJ, Schaffer JE Fatigue performance of Resoloy® magnesium alloy wire. Eur Cells Mater
23. WilliamM. Steen · JyotirmoyMazumder LaserMaterial Processing 4th Edition
24. Hagemann HJ, Gudat W, Kunz C (1975) Optical constants from the far infrared to the x-ray region: Mg, Al, Cu, Ag, Au, Bi, C, and Al2O3. J Opt Soc Am 65:742–744
25. www.goodfellow.com
26. www.nist.gov
27. Demir AG (2019) Single track deposition study of biodegradable Mg-rare earth alloy by micro laser metal wire deposition. Mater Today Proc 7:426–434 . doi: 10.1016/j.matpr.2018.11.105
28. Biffi CA, Tuissi A, Demir AG (2021) Martensitic transformation, microstructure and functional behavior of thin-walled Nitinol produced by micro laser metal wire deposition. J Mater Res Technol 12:2205–2215 . doi: 10.1016/j.jmrt.2021.03.108
29. Demir AG (2018) Micro laser metal wire deposition for additive manufacturing of thin-walled structures. Opt Lasers Eng 100: . doi: 10.1016/j.optlaseng.2017.07.003
30. Demir AG, Previtali B, Biffi CA (2013) Fibre Laser Cutting and Chemical Etching of AZ31 for Manufacturing Biodegradable Stents. Adv Mater Sci Eng 2013:1–11 . doi: 10.1155/2013/692635
31. Demir AG, Biffi CA (2019) Micro laser metal wire deposition of thin-walled Al alloy components: Process and material characterization. J Manuf Process 37:362–369 . doi: 10.1016/j.jmapro.2018.11.017
32. Carroll BE, Palmer TA, Beese AM (2015) Anisotropic tensile behavior of Ti-6Al-4V components fabricated with directed energy deposition additive manufacturing. Acta Mater. doi: 10.1016/j.actamat.2014.12.054
33. Demir AG, Biffi CA (2019) Micro laser metal wire deposition of thin-walled Al alloy components: Process and material characterization. J Manuf Process 37: . doi: 10.1016/j.jmapro.2018.11.017
34. Wu H, Huang Q, Ren J, et al (2017) Novel Mg-based alloys by selective laser melting for biomedical applications: microstructure evolution, microhardness and in vitro degradation behaviour . Virtual Phys Prototyp 13:71–81 . doi: 10.1080/17452759.2017.1411662
35. Zhang B, Liao H, Coddet C (2012) Effects of processing parameters on properties of selective laser melting Mg-9%Al powder mixture. Mater Des 34:753–758 . doi: 10.1016/j.matdes.2011.06.061
36. Wei K, Gao M, Wang Z, Zeng X (2014) Effect of energy input on formability, microstructure and mechanical properties of selective laser melted AZ91D magnesium alloy. Mater Sci Eng A 611:212–222 . doi: 10.1016/j.msea.2014.05.092
37. Wei K, Wang Z, Zeng X (2015) Influence of element vaporization on formability, composition, microstructure, and mechanical performance of the selective laser melted Mg-Zn-Zr components. Mater Lett 156:187–190 . doi: 10.1016/j.matlet.2015.05.074
38. Shuai C, Yang Y, Wu P, et al (2017) Laser rapid solidification improves corrosion behavior of Mg-Zn-Zr alloy. J Alloys Compd 691:961–969 . doi: 10.1016/j.jallcom.2016.09.019
39. Montani M, Demir AG, Mostaed E, et al (2017) Processability of pure Zn and pure Fe by SLM for biodegradable metallic implant manufacturing. Rapid Prototyp J 23:514–523 . doi: 10.1108/RPJ-08-2015-0100
40. Liu C, Zhang M, Chen C (2017) Effect of laser processing parameters on porosity, microstructure and mechanical properties of porous Mg-Ca alloys produced by laser additive manufacturing. Mater Sci Eng A 703:359–371 . doi: 10.1016/j.msea.2017.07.031
41. Mostaed E, Vedani M, Hashempour M, Bestetti M (2014) Influence of ECAP process on mechanical and corrosion properties of pure Mg and ZK60 magnesium alloy for biodegradable stent applications. Biomatter 4:e28283 . doi: 10.4161/biom.28283

List of figures

List of tables